THE JOURNAL OF PHYSICAL CHEMISTRY C

Article

Cite This: J. Phys. Chem. C 2018, 122, 27567−27574

pubs.acs.org/JPCC

Band Engineering of $SrTiO_3$: Effect of Synthetic Technique and Site Occupancy of Doped Rhodium

U. Sandhya Shenoy,[†,‡] Harsha Bantawal,[†] and D. Krishna Bhat*[,†]

[†]Department of Chemistry, National Institute of Technology Karnataka, Surathkal, Mangalore 575025, India

[‡]Department of Chemistry, College of Engineering and Technology, Srinivas University, Mukka, Mangalore 574146, India

Supporting Information

ABSTRACT: It is well known that doping of Rh into the $SrTiO_3$ lattice introduces 4d donor levels within the band gap, which causes reduction in the gap and extends the photocatalytic activity to the visible region of the solar spectrum. The mid-gap states formed also act as recombination centers and diminish the efficiency of the material. Herein, we present a combined theoretical and experimental approach to avoid the formation of the so-called acceptor mid-gap states. For the first time, we study the effect of occupancy of Rh in the Sr site. First-principles calculations reveal that mixed occupancies of Rh into Sr and Ti sites lead to the introduction of acceptor levels within the band gap, leading to decrease in photocatalytic efficiency. A facile one-pot solvothermal approach by avoiding high-temperature calcinations is reported to obtain Rh-doped $SrTiO_3$ nanoparticles in Rh^{3+} states, suppressing the formation of Rh^{4+} states by directing Rh toward Sr sites. The photocatalytic activity of Rh-doped $SrTiO_3$ nanoparticles is studied in the case of degradation of methylene blue, wherein the 1.0 Rh sample was found to be highly efficient.

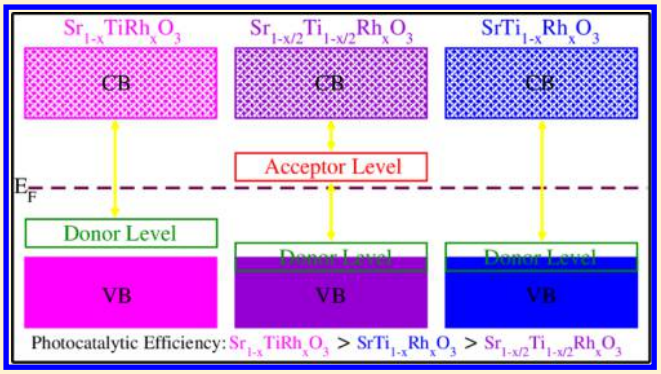

INTRODUCTION

Photocatalysis has been considered the most realistic solution for solving environmental pollution because of its ability to degrade pollutants by an economic, nontoxic, and environmentally friendly procedure.[1] An ideal photocatalyst should have a band gap which allows absorption of visible light; nil or very low recombination rate of charge carriers and high stability in the working environment.[2] Various metal oxide semiconductors, such as TiO_2, ZnO, Fe_3O_4, $FeWO_4$, $NiWO_4$, $SrTiO_3$, $BaTiO_3$, and $CaTiO_3$, have been employed as photocatalysts but they suffer a major drawback because of their large band gap (≥3.2 eV), which restricts their absorption to the ultraviolet range, occupying only a very small fraction of the solar spectrum.[3−10] An effective strategy to extend the absorption into the visible region is by doping various elements into the host lattice of these oxide materials.

$SrTiO_3$ is an attractive candidate for the photocatalytic degradation of organic pollutants because of its excellent structural stability, photocorrosion resistivity, and electronic structure tunability. Several approaches have been explored in order to reduce the band gap of $SrTiO_3$, especially by doping with a metal or nonmetal element. Because there are three possible sites for doping namely, Sr, Ti, and O site, various elements, such as M = Ag, Bi, Co, Cr, Fe, Ir, La, Mn, Nb, Pb, Pd, Pt, Rh, Ru, Sb, and Zn have been utilized for Sr or/and Ti site doping and codoping, whereas B, N, and F have been used for substitution at the O site either alone or accompanied by M doping in Sr/Ti sites.[11−24] Among these, Rh-doped $SrTiO_3$ has attracted significant attention because of its absorption in the visible region.[22,23,25−30] When Rh is doped into $SrTiO_3$, both Rh^{3+} and Rh^{4+} exist in the lattice.[27,28] Though Rh doping decreases the band gap of the material because of Rh^{3+} states acting as donor levels, it suffers from the drawback that acceptor states get formed in the mid-gap region because of the presence of Rh^{4+} states.[22,27,28] Doping Rh by maintaining it in the +3 state, by avoiding the formation of photocatalytically inactive +4 state, has become a challenge in the synthesis of Rh-doped $SrTiO_3$.

In this paper, for the first time we carry out density functional theory (DFT) electronic structure calculations for Rh in the Sr site along with the well-known Ti-site occupancy. The first-principles calculations reveal that the mixed occupancy of Sr and Ti sites by the Rh dopant leads to the formation of unfavorable acceptor states, which act as the recombination center diminishing the photocatalytic efficiency of the material. Hence, designing the synthetic technique to direct Rh into either Sr or Ti site only can avoid the formation of acceptor states because of the Rh orbital. In support, we report synthesis of Rh-doped $SrTiO_3$ nanoparticles by a facile one pot solvothermal method by avoiding high-temperature calcinations, which directs Rh into the Sr site. Rh is found to be in the

Received: October 16, 2018
Revised: November 17, 2018
Published: November 19, 2018

DOI: 10.1021/acs.jpcc.8b10083
J. Phys. Chem. C 2018, 122, 27567−27574

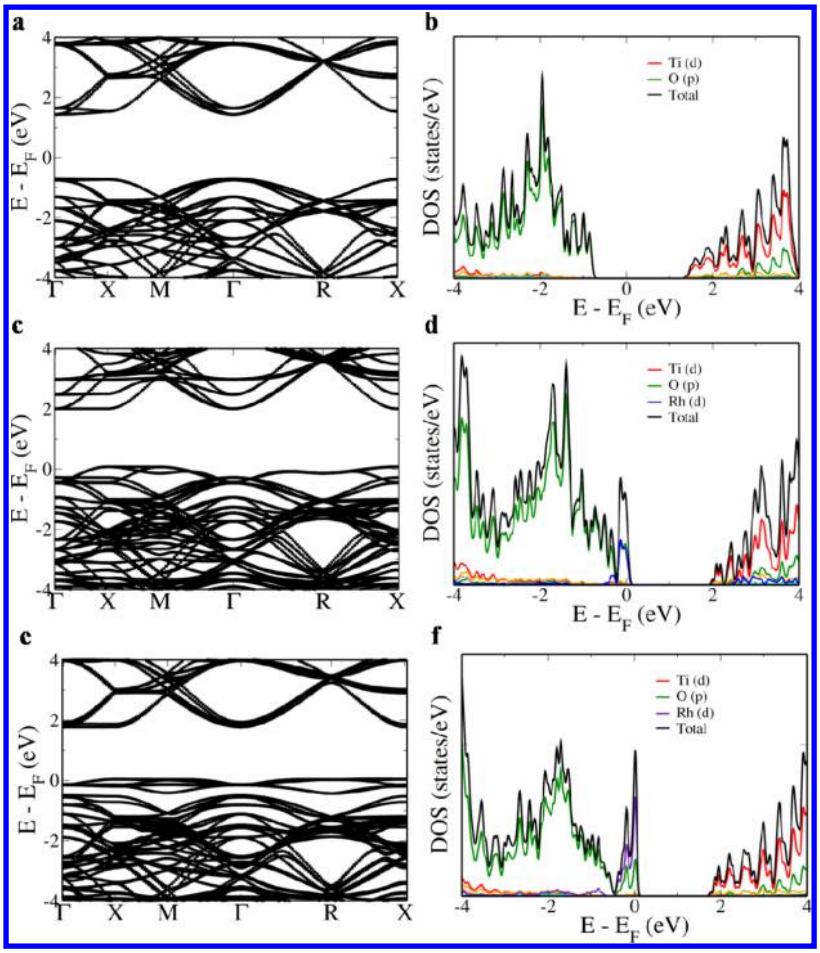

Figure 1. (a) Electronic structure and (b) pdos of the 2 × 2 × 2 supercell of $SrTiO_3$, (c) electronic structure and (d) pdos of the 2 × 2 × 2 supercell of Rh-doped $SrTiO_3$ with Rh in the Ti site, (e) electronic structure and (f) pdos of the 2 × 2 × 2 supercell of Rh-doped $SrTiO_3$ with Rh in the Sr site.

+3 oxidation state, as the formation of unwanted Rh^{4+} state is suppressed under the synthetic conditions employed. The photocatalytic activity of Rh-doped $SrTiO_3$ nanoparticles was evaluated by taking MB as a target pollutant.

METHODS

Computational Details. Open source computer code Quantum ESPRESSO suite based on DFT was used to carry out electronic structure calculations of pristine $SrTiO_3$ and Rh-doped $SrTiO_3$.[31] The electron wavefunctions were described by nonrelativistic Martins−Troullier norm-conserving pseudopotentials. Local density approximation to approximate the exchange−correlation energy functional of Perdew−Wang functional type was used. $5s^2$, $3d^24s^2$, $2s^22p^4$, and $4d^85s^1$ valence electrons of Sr, Ti, O, and Rh, respectively, were included in the first-principles calculations. 40 atoms' supercell (2 × 2 × 2) of primitive cubic perovskite $SrTiO_3$, was considered for the current study.[32] All the simulations were carried out using fully relaxed structures with a wavefunction energy cutoff of 80 Ry and a charge density cutoff of 320 Ry. A *k*-mesh of 4 × 4 × 4 for self consistent field calculations and 8 × 8 × 8 for nonself-consistent field calculations was made use of. A path following the Γ−*X*−*M*−Γ−*R*−*X* order of high symmetry points in the Brillouin zone was used for the determination of electronic structure.

Synthesis. All chemicals were of analytical grade and were used as procured (Sigma-Aldrich) without any purification. Rh-doped $SrTiO_3$ with varying percentage of Rh was synthesized as follows: 1.47 mL of titanium(IV) isopropoxide and rhodium(III) chloride were dissolved in 10 mL of 2-propanol, which was labeled solution A. An appropriate amount of strontium nitrate was dissolved in 10 mL of 2 M KOH, which was labeled solution B. Solution A was continuously stirred, as solution B was added dropwise to it. The resulting mixture was transferred to an autoclave and heated in an oven at 200 °C for 4 h. The obtained precipitate was first purified by washing with 1 M acetic acid and water and then dried in an oven at 70 °C for 8 h. The products finally obtained by taking 0.1, 0.5, 1.0, and 3.0 mol % of the Rh precursor were designated as 0.1 Rh, 0.5 Rh, 1.0 Rh, and 3.0 Rh, respectively.

Characterization. The structure of the prepared catalyst was determined using a Rigaku X-ray diffractometer (XRD) with monochromatic Cu Kα radiation (λ = 0.154 nm) in the range of 20−80° at a scan rate of 2° per minute. The morphology of the sample was analyzed using a Carl Zeiss field emission scanning electron microscope (FESEM) and FEI Tecnai transmission electron microscope (TEM). The elemental composition was determined using an Oxford energy-dispersive X-ray (EDX) analysis instrument. The X-ray photoelectron spectrum (XPS) was collected on a Kratos XSAM800 spectrometer equipped with an Al Kα source. Diffuse reflectance (DR) spectrum was recorded using an Analytic Jena UV−visible DR spectrometer. The photoluminescence (PL) spectrum was obtained using a HORIBA Jobin Yvon fluorescence spectrometer.

DOI: 10.1021/acs.jpcc.8b10083
J. Phys. Chem. C 2018, 122, 27567−27574

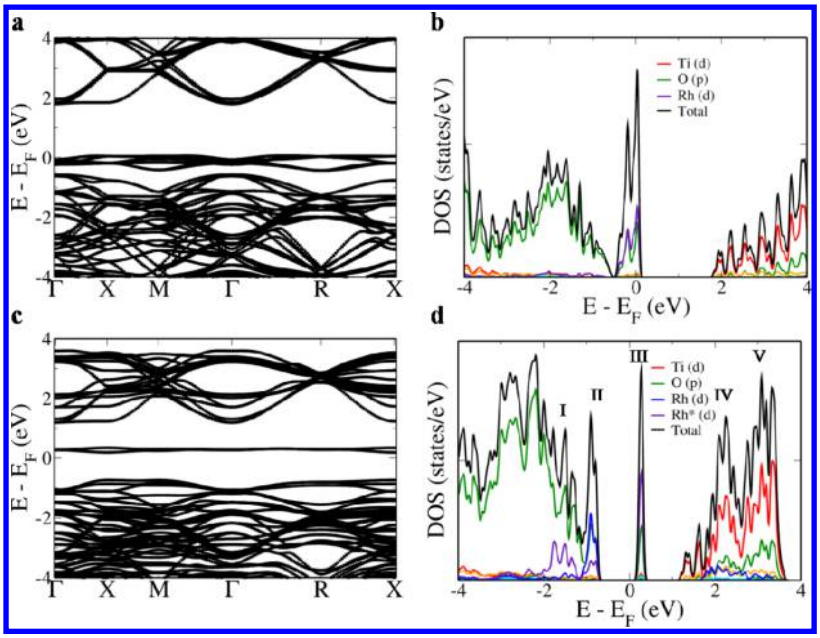

Figure 2. (a) Electronic structure and (b) pdos of the 2 × 2 × 2 supercell of Rh-doped $SrTiO_3$ with two Rh in Sr sites, (c) electronic structure and (d) pdos of the 2 × 2 × 2 supercell of Rh-doped $SrTiO_3$ with one Rh in the Ti site (blue) and another Rh in the Sr site (lavender) indicated as Rh*.

Determination of Photocatalytic Activity. The photocatalytic studies were carried out using a reactor equipped with a high-pressure 250 W Hg vapor lamp acting as a visible light source (λ = 410−700 nm). In a 500 mL pyrex glass beaker, 100 mL of solution containing 1 mg of MB and 50 mg of photocatalyst was magnetically stirred for 30 min to achieve the adsorption−desorption equilibrium of the catalyst. Later, the visible light irradiated solution was drawn out at regular intervals in quantity of 5 mL and centrifuged. The supernatant solution was subjected to DR analysis at 664 nm. Considering C_o as the initial concentration of the solution and C as the concentration at different intervals of time, the percentage degradation of dye is given by eq 1.

$$\text{Degradation } \% = [(C_o - C)/C_o] \times 100 \quad (1)$$

RESULTS AND DISCUSSION

Results from First-Principles Calculation. The cubic perovskite structure of $SrTiO_3$ consists of a Ti atom at the center with Sr atoms occupying the corner. O atoms, on the other hand occupy the face center. The electronic structure of 2 × 2 × 2 supercell of the primitive $SrTiO_3$ shown in Figure 1a reveals a direct band gap of 2.137 eV at the Γ point with O p orbitals forming the valence band and Ti d orbitals constituting the conduction band states as revealed by the partial density of states (pdos) plot (Figure 1b). This band gap is consistent with the indirect band gap estimate of 2.14 eV from the $R \rightarrow \Gamma$ point of the primitive cell reported earlier.[33] This is caused because of folding of bands in the current supercell, which is well documented in the literature.[33,34] The decrease in the estimated band gap is in line with the typical underestimation, resulting in DFT calculations.[33,34] When $SrTiO_3$ is doped with Rh, Rh can occupy either Sr site or Ti site (Figure S1). It is seen that the estimated lattice constant decreases to 3.7633 Å when Rh occupies the Sr site, while it increases to 3.8327 Å when it occupies the Ti site from the estimated theoretical equilibrium lattice constant of 3.8128 Å of pure $SrTiO_3$. These results support the data from XRD analysis given in the next section, confirming that in the present study Rh occupies the Sr site. When the Rh atom substitutes the Ti site, the band gap decreases to 1.926 eV at the X point (Figure 1c) because of the appearance of a donor level which overlaps with the valence band edge elevating the valence band maximum (VBM). This donor level is constituted by Rh d states hybridized with O p states (Figure 1d).[20] The Fermi level shifting toward the valence band makes Rh-doped $SrTiO_3$ a p-type material.

Because there are no reports on the modification of electronic structure when Rh occupies the Sr site, one of the Sr atom was replaced with the Rh atom and simulation was carried out. In this case, the Rh d states appear as a separate level at 0.069 eV above the VBM but within the Fermi level indicating the donor nature (Figure 1e). The appearance of donor level decreases the band gap and increases the visible light absorption efficiency. The gap between the top of the donor level and the conduction band maximum is found to be 1.822 eV with the width of the donor band being 0.485 eV (Figure 1f). In both the cases of Rh in the Ti site or Sr site, the donor level resembles the states caused because of Rh^{3+} as reported earlier.[27] The continuous nature of the band structure at the edges (as revealed by the pdos plot) facilitates easy migration of photogenerated carriers, thereby increasing the efficiency. Because the defect band is only slightly above the valence band, after the excitation process, rapid replenishment of electrons is possible, thus avoiding the vacant dopant states from becoming traps for the electrons in the conduction band.[29]

When concentration of Rh is doubled, similar features appear (Figures S2 and 2). When two Sr sites are occupied by Rh atoms, the band gap decreases further to 1.731 eV with the increase in the width of the defect band to 0.499 eV (Figure 2a). The defect level appears 0.132 eV above the VBM with the increase in the intensity of the density of states in that region (Figure 2b). The pdos plot reveals strong hybridization between the O p states which constitutes the valence band and the Rh d states of the dopant atom, which is very essential for achieving a high activity as it strongly affects the photocarrier lifetime and mobility.[20,27]

DOI: 10.1021/acs.jpcc.8b10083
J. Phys. Chem. C 2018, 122, 27567−27574

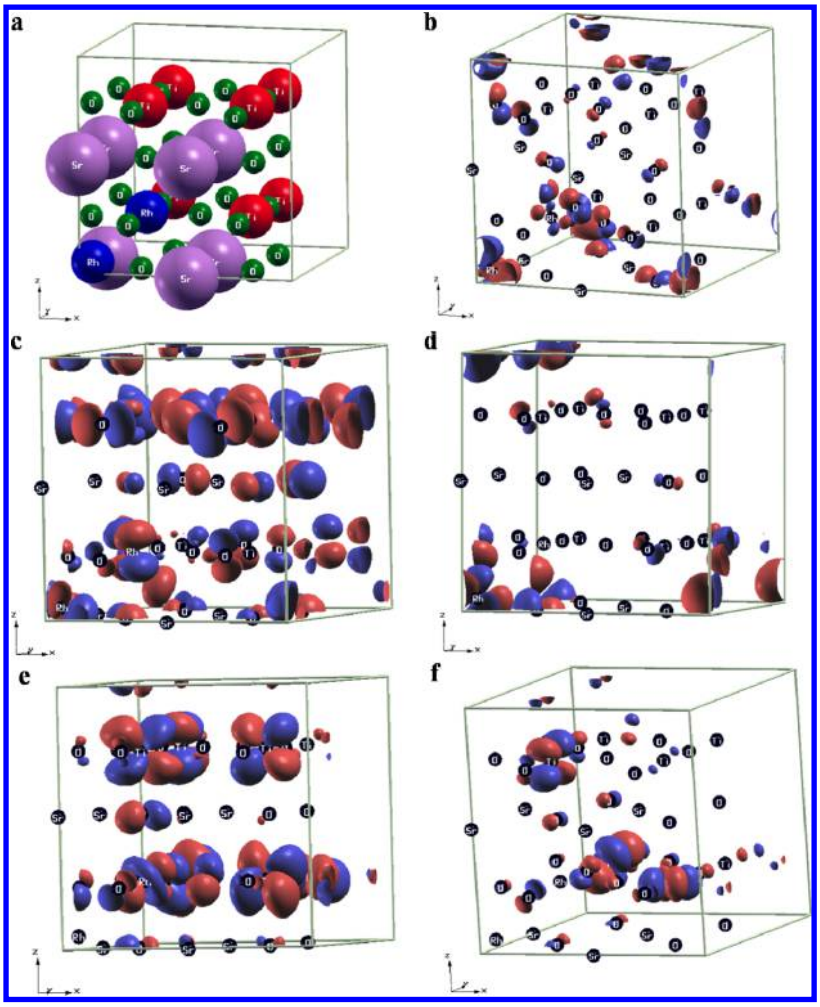

Figure 3. (a) Crystal structure of the 2 × 2 × 2 supercell of Rh-doped $SrTiO_3$ with one Rh in the Ti site and another Rh in the Sr site. Wavefunction visualization at the Γ point (b−f) corresponding to various energy levels as indicated by Roman numerals I−V in the pdos in Figure 2d, respectively. Red and blue colors in (b−f) indicate the positive and negative lobes of the orbitals.

To understand the nature of electronic structure in the case of mixed doping, one of the Sr atoms and one of the Ti atoms were substituted with Rh atoms each (Figure 3a). The electronic structure reveals two in-gap features (Figure 2c,d). Visualization of the wavefunctions at Γ point corresponding to 1.5 eV below the Fermi level (indicated by I, in Figure 2d) reveals that the major contribution is from the O p states followed by contribution from the d orbitals of Rh-substituted at the Sr site with a minor contribution from the d orbitals of Rh-substituted at the Ti site (Figure 3b). The Rh atom substituted for the Ti atom introduces a donor level which overlaps with the VBM, making the band gap reduced to 1.926 eV as in the case of single Rh atom substituted in the Ti site mentioned earlier. The presence of this impurity donor level (indicated by II, in Figure 2d) closer to the VBM suppresses the photocarrier localization at the impurity sites. At this energy level, the contribution from the d orbitals of Rh-substituted at Ti site is found to be higher than that from Rh-substituted at the Sr site (Figure 3c).

The Rh atom substituted in the Sr site introduces an acceptor level 0.926 eV above the VBM (Figure 2c,d). This is also supported by the results given in Figure 3d, which shows maximum contribution to the acceptor level (indicated by III, in Figure 2d) from the d orbitals of Rh substituted at the Sr site along with the O p orbitals and zero contribution from the orbitals of Rh-substituted at the Ti site. The presence of this acceptor level at mid-gap position sharply decreases the photocarrier lifetime as it acts as an electron−hole recombination center similar to the one introduced by Rh^{4+} states in earlier reports.[27] As revealed in Figures 2d and 3e,f, the conduction band is formed by major contributions from the d orbitals of Ti with the p orbitals of O showing minor contribution. Around ∼2 eV above the Fermi level (indicated by IV, in Figure 2d) we see minor contributions from the d orbitals of Rh-substituted at the Ti site (Figure 3e), whereas beyond ∼3.5 eV above the Fermi level (indicated by V, in Figure 2d) the contributions from the Rh orbitals vanishes (Figure 3f). The large gap between the VBM and the acceptor states inhibit the replenishment of electrons and hence the vacant states can be replenished only by absorbing additional photons, leading to larger lifetime of the recombination center.[29] Therefore, it is safe to assume that Rh atoms occupying a single type of site introduces only donor states, whereas mixed site occupancy results in the introduction of recombination centers.

Because the current synthetic technique directs Rh toward the Sr site discussed in subsequent sections, the 2 × 2 × 1 supercell was used to simulate higher doping concentration with a *k*-mesh of 12 × 12 × 24 and 24 × 24 × 48 for scf and nscf calculations, respectively. Two of the Sr atoms in this cell were replaced with two Rh atoms which resulted in the decrease in band gap to 1.069 eV at the Γ point. The increase in concentration of Rh

DOI: 10.1021/acs.jpcc.8b10083
J. Phys. Chem. C 2018, 122, 27567−27574

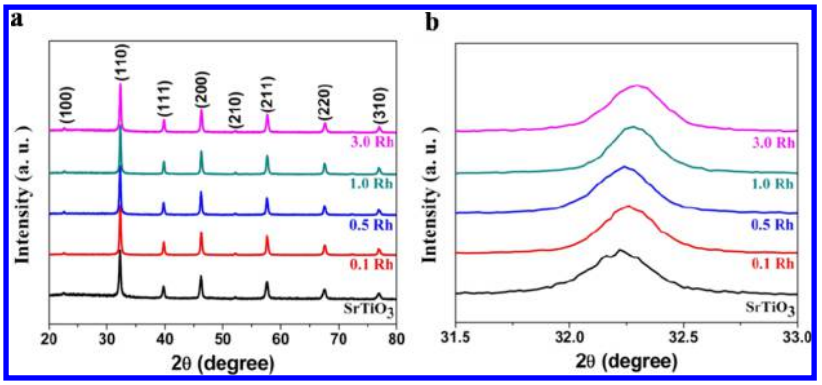

Figure 4. (a) XRD patterns as a function of doping concentrations of Rh and (b) diffraction peaks of (110) planes in the range of $2\theta = 31.5-33°$.

doping in $SrTiO_3$ results in the decrease in the band gap, which is consistent with the experimental results, extending the absorption curve toward the visible region of the solar spectrum. Further, an increase in the width of the defect band to 1.069 eV with slight overlap at the Z point was also seen consistent with the above reported trend (Figure S3). These results suggests that a single type of occupancy of Rh dopants in the $SrTiO_3$ lattice is favorable for enhancing the photocatalytic efficiency as it introduces only donor states unlike mixed occupancies which introduces recombination centers detrimental to its application in photocatalysis.

XRD Analysis. The XRD patterns of the $SrTiO_3$ and Rh-doped $SrTiO_3$ (Figure 4a) could be indexed to the cubic phase of $SrTiO_3$ with JCPDS card number 01-089-4934. Absence of impurity peaks indicates that Rh occupied the lattice sites of the host structure. The similarity of the patterns of doped samples with that of pristine indicates that the overall crystal structure was not much affected by the doping in the concentration range studied. It was observed that (110) peaks appearing in the 2θ range of 32−32.5° of the doped samples (Figure 4b) shifted toward higher θ values, which caused a decrease in the lattice parameter from 3.971 to 3.941 Å. This could be a consequence of Rh substituting Sr as the ionic radius of Rh^{3+} (0.067 nm) is smaller than Sr^{2+} (0.118 nm). Rh replacing Ti would have increased the lattice constant as Ti^{4+} (0.061 nm) is small, consistent with the theoretical results explained in the previous section.

FESEM, TEM, and EDX Analysis. The FESEM image of 1.0 Rh sample (Figure 5a) revealed numerous irregular spherical

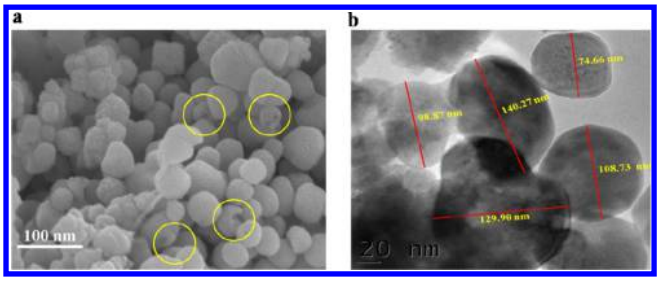

Figure 5. (a) FESEM image and (b) TEM image of 1.0 Rh.

particles which are highly porous. Some broken spheres indicate the hollow nature of the material (circled yellow). Efficient photocatalysis requires a large contact area between the catalyst material and the reactant species, in addition to the visible light absorption. The spherical particle is known to provide high surface area and in addition to it the porous nature of the doped samples with low density offers large interaction frequency and high-speed molecular transport. The TEM image (Figure 5b) reveals irregular spherical particles with their average size ranging from 70 to 150 nm. EDX analysis (Figure S4a) reveals the presence of Sr, Ti, O, and Rh, indicating the successful doping. The selected area electron diffraction (SAED) pattern (Figure S4b) shows the presence of discrete diffraction spots which confirms the polycrystalline nature of the sample and these spots corresponding to (220), (200), and (110) planes of the cubic phase of $SrTiO_3$ is in good agreement with the XRD results.

XPS Analysis. XPS was used to analyze the surface chemical composition of Rh-doped samples. Figure S5 shows the full range XPS survey plot of the as-synthesized 1.0 Rh sample. The deconvoluted spectra (Figure 6a) show peaks with binding energies of 132.31 and 133.96 eV which can be attributed to Sr $3d_{5/2}$ and Sr $3d_{3/2}$ states, respectively. The peaks with binding energies of 457.5 and 463.3 eV (Figure 6b) can be indexed to Ti $2p_{3/2}$ and Ti $2p_{1/2}$ states, respectively. These binding energy values correspond to Ti with the oxidation state of 4+ in the perovskite structure of $SrTiO_3$.[30] Figure 6c shows the high resolution O 1s spectrum which can be deconvoluted into two peaks of binding energies 528.83 and 530.75 eV which can be allotted to oxygen in the oxide lattice (O_L) and surface hydroxyl groups (O_{OH}), respectively. The peaks shown in Figure 6d with binding energies of 308.5 and 313.1 eV can be indexed to Rh $3d_{5/2}$ and Rh $3d_{3/2}$ states, respectively corresponding to Rh with 3+ oxidation states.[30] The absence of peaks corresponding to Rh^{4+} states indicates the successful incorporation of Rh into $SrTiO_3$ as Rh^{3+} and not as Rh^{4+}.

Optical Absorbance Analysis. The DR spectra were measured as a function of wavelength from 250 to 700 nm (Figure 7a) which shows increase in intensity of absorption in the 400 to 500 nm range and thereafter a steady absorption with increase in the concentration of Rh in $SrTiO_3$.[16,30] Further, the spectra did not show any presence of the characteristic absorption peak at 580 nm, caused by Rh^{4+}, indicating the absence of this species in the sample.[27] The Tauc relation was used to calculate the direct band gap of the samples using eq 2.[2,35]

$$(\alpha h\nu)^2 = K(h\nu - E_g) \tag{2}$$

where α is the absorption coefficient, E_g is the band gap energy of the semiconductor, K is a constant, and $h\nu$ is the photon energy. The band gap energies of $SrTiO_3$, 0.1 Rh, 0.5 Rh, 1.0 Rh, and 3.0 Rh were found to be 3.24, 3.01, 2.55, 2.42, and 2.0 eV, respectively (Figure 7b). The absorption edge is seen to increase

DOI: 10.1021/acs.jpcc.8b10083
J. Phys. Chem. C 2018, 122, 27567−27574

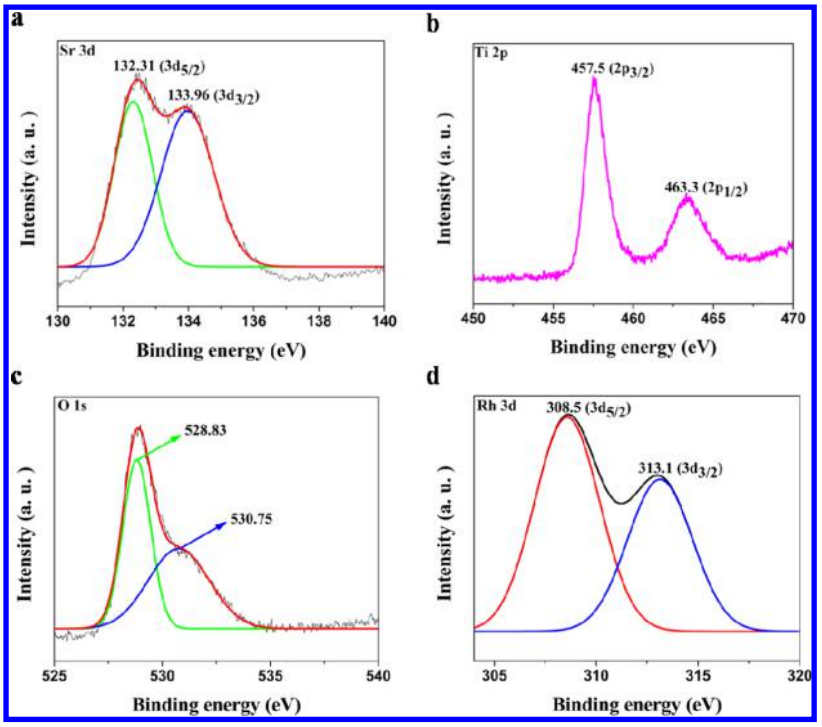

Figure 6. High-resolution XPS plot of (a) Sr 3d, (b) Ti 3p, (c) O 1s, and (d) Rh 3d.

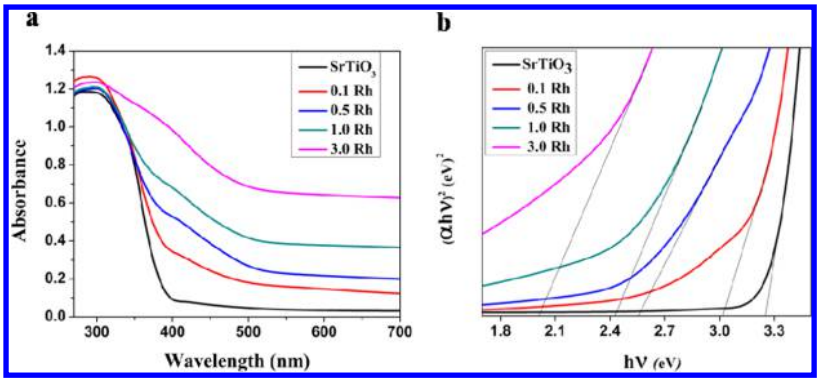

Figure 7. (a) UV−visible DR spectra and (b) Tauc plots of $SrTiO_3$ and Rh-doped $SrTiO_3$ samples.

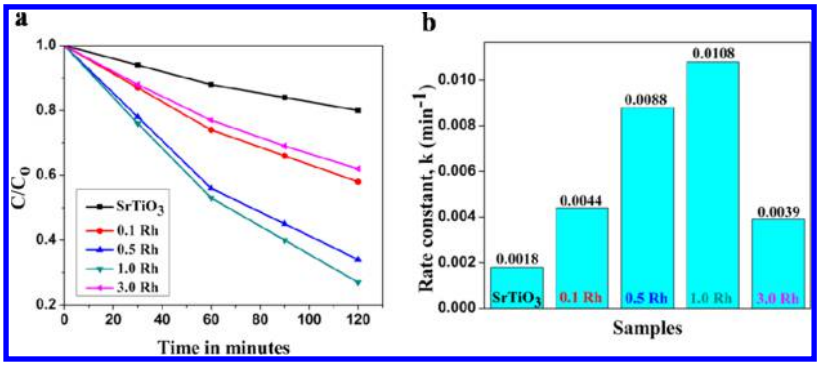

Figure 8. (a) Photocatalytic degradation of MB and (b) the rate constants of the photocatalytic degradation of MB by the synthesized $SrTiO_3$ and Rh-doped $SrTiO_3$.

beyond 385 nm as the concentration of Rh is increased. The decrease in the band gap with the red shift in the absorption peak points to the formation of donor levels in the doped samples.[29]

Figure S6 shows the comparison of the PL spectra of $SrTiO_3$ and Rh-doped samples. The decrease in the intensity of the doped sample is because of the lower rate of recombination of electrons and holes because of the rapid rate of replenishment of electrons to the vacant site by the valence band as discussed in the DFT results. This indirectly supports the fact that Rh atoms have only single type of occupancy till 1.0 Rh. For 3.0 Rh, the

DOI: 10.1021/acs.jpcc.8b10083
J. Phys. Chem. C 2018, 122, 27567−27574

intensity of PL is higher than the 1.0 Rh sample, indicating that acceptor states are formed for this particular doping amount, which may be because of mixed occupancy at higher concentrations of Rh.

Photocatalytic Activity. MB was chosen as a target moiety for testing the photocatalytic efficiency of Rh-doped samples. The percentage degradation of $SrTiO_3$, 0.1 Rh, 0.5 Rh, 1.0 Rh, and 3.0 Rh was found to be 20, 41.6, 65.2, 72.9, and 37.5, respectively (Figure 8a). The results indicate that with the increase in Rh content the photocatalytic efficiency increases but beyond 1.0 Rh, the photocatalytic activity decreases. This could be because of the fact that though the band gap decreases with the increase in concentration of Rh as calculated by DFT, with the increase in concentration of Rh there is a possibility of mixed occupancy of sites because of which acceptor levels generated lead to the recombination of photogenerated charge carriers which is also supported by the results from PL. The above photocatalysis reaction follows the first-order rate equation as given in eq 3.[6,35]

$$\ln(C/C_o) = -kt \quad (3)$$

where, C_o is the concentration of dye at time $t = 0$, C is the concentration of the dye at irradiation time "t", and k is the first-order rate constant, given by the slope of the straight line. The 1.0 Rh sample exhibited a highest rate constant of 0.0108 min^{-1} compared to $SrTiO_3$, which showed a value of 0.0018 min^{-1} (Figure 8b). The catalyst showed only a slight decline in the activity even after four cycles, indicating its stability and reusability for practical applications (Figure S7). To further confirm the stability of the material, we obtained the XRD patterns of the 1.0 Rh sample after the photocatalytic measurements and compared it with the freshly synthesized sample. Figure S8 shows the XRD patterns of the unused and the used (after four cycles) 1.0 Rh samples. It is clear from the figure that the pattern corresponding to the used sample after four cycles exactly resembles to that of the unused one. Further, there are no extra or impurity peaks, suggesting that the sample has not undergone any degradation indicating the stability of the sample.

Photocatalytic Reaction Mechanism. The Rh-doped $SrTiO_3$ exhibited higher photocatalytic activity as compared to undoped $SrTiO_3$ because of the formation of donor levels by the Rh d orbitals which lie slightly above the VBM, thus reducing the band gap.[27] When 1.0 Rh was exposed with the energy of photon equal to or greater than its band gap, the electron from the donor level is transferred to the conduction band and these electrons react with oxygen to produce superoxide radicals. Meanwhile, the formed holes either directly react with MB or with water molecules to produce hydroxyl radicals. These two radicals are said to be active species for the effectual degradation of MB to harmless degradation products (Figure 9).

CONCLUSIONS

A combined theoretical and experimental approach was used to improve the photocatalytic activity of $SrTiO_3$ nanoparticles via doping Rh. First-principles DFT calculations revealed that if Rh occupies either Sr or Ti sites with a single type of occupancy then, only donor states are formed which decreases the band gap and extends the absorption to the visible region of the solar spectrum. Mixed occupancies lead to the introduction of acceptor levels which act as recombination centers, which decrease the photocatalytic efficiency. A facile one-pot solvothermal approach was used to synthesize Rh-doped $SrTiO_3$ nanoparticles by avoiding high-temperature calcinations where in Rh is directed to the Sr site. The samples were thoroughly characterized by various techniques which confirm the presence of Rh in the 3+ state. The 1.0 Rh sample was found to be highly active for the photocatalytic degradation of MB dye.

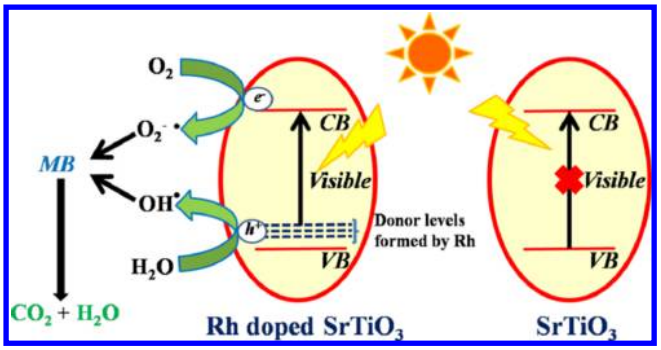

Figure 9. Photocatalytic mechanism of Rh-doped $SrTiO_3$ for the degradation of MB under visible-light irradiation.

ASSOCIATED CONTENT

Supporting Information

The Supporting Information is available free of charge on the ACS Publications website at DOI: 10.1021/acs.jpcc.8b10083.

Crystal structure of 2 × 2 × 2 supercells, electronic structure and pdos of Rh-doped $SrTiO_3$ of different configurations, EDX plot, SAED pattern, full range XPS plot of the 1.0 Rh sample, PL spectra, reusability plot, and XRD patterns of the 1.0 Rh sample (PDF)

AUTHOR INFORMATION

Corresponding Author

*E-mail: denthajekb@gmail.com.

ORCID

D. Krishna Bhat: 0000-0003-0383-6017

Notes

The authors declare no competing financial interest.

ACKNOWLEDGMENTS

H.B. is grateful to the National Institute of Technology Karnataka Surathkal, Mangalore, for providing financial support and facilities to carry out this research work.

REFERENCES

(1) Zhao, L.; Deng, J.; Sun, P.; Liu, J.; Ji, Y.; Nakada, N.; Qiao, Z.; Tanaka, H.; Yang, Y. Nanomaterials for treating emerging contaminants in water by adsorption and photocatalysis: systematic review and bibliometric analysis. *Sci. Total Environ.* **2018**, *627*, 1253−1263.

(2) Sadiq, M. M. J.; Shenoy, U. S.; Bhat, D. K. Synthesis of BaWO4/NRGO-g-C3N4 nanocomposites with excellent multifunctional catalytic performance via microwave approach. *Front. Mater. Sci.* **2018**, *12*, 247−263.

(3) Humayun, M.; Raziq, F.; Khan, A.; Luo, W. Modification strategies of TiO_2 for potential applications in photocatalysis: a critical review. *Green Chem. Lett. Rev.* **2018**, *11*, 86−102.

(4) Grabowskaa, E.; Diak, M.; Klimczuk, T.; Lisowski, W.; Zaleska-Medynska, A. Novel decahedral TiO2 photocatalysts modified with Ru or Rh NPs: insight into the mechanism. *Mol. Catal.* **2017**, *434*, 154−166.

(5) Ong, C. B.; Ng, L. Y.; Mohammad, A. W. A review of ZnO nanoparticles as solar photocatalysts: synthesis, mechanisms and applications. *Renewable Sustainable Energy Rev.* **2018**, *81*, 536−551.

DOI: 10.1021/acs.jpcc.8b10083
J. Phys. Chem. C 2018, 122, 27567−27574

(6) Sadiq, M. M. J.; Shenoy, U. S.; Bhat, D. K. Enhanced photocatalytic performance of N-doped RGO-$FeWO_4$/Fe_3O_4 ternary nanocomposite in environment applications. *Mater. Today Chem.* **2017**, *4*, 133−141.
(7) Sadiq, M. M. J.; Shenoy, U. S.; Bhat, D. K. Novel RGO-$ZnWO_4$-Fe_3O_4 nanocomposite as high performance visible light photocatalyst. *RSC Adv.* **2016**, *6*, 61821−61829.
(8) Sadiq, M. M. J.; Shenoy, U. S.; Bhat, D. K. $NiWO_4$-ZnO-NRGO ternary nanocomposite as an efficient photocatalyst for degradation of methylene blue and reduction of 4-nitro phenol. *J. Phys. Chem. Solids* **2017**, *109*, 124−133.
(9) Wang, W.; Tadé, M. O.; Shao, Z. Research progress of perovskite materials in photocatalysis- and photovoltaics-related energy conversion and environmental treatment. *Chem. Soc. Rev.* **2015**, *44*, 5371−5408.
(10) Zhang, G.; Liu, G.; Wang, L.; Irvine, J. T. S. Inorganic perovskite photocatalysts for solar energy utilization. *Chem. Soc. Rev.* **2016**, *45*, 5951−5984.
(11) Zhang, Q.; Huang, Y.; Xu, L.; Cao, J.-j.; Ho, W.; Lee, S. C. Visible-light-active plasmonic Ag-SrTiO3 nanocomposites for the degradation of NO in air with high selectivity. *ACS Appl. Mater. Interfaces* **2016**, *8*, 4165−4174.
(12) Irie, H.; Maruyama, Y.; Hashimoto, K. Ag+ - and Pb2+ -doped SrTiO3 photocatalysts. A correlation between band structure and photocatalytic activity. *J. Phys. Chem. C* **2007**, *111*, 1847−1852.
(13) Lv, M.; Xie, Y.; Wang, Y.; Sun, X.; Wu, F.; Chen, H.; Wang, S.; Shen, C.; Chen, Z.; Ni, S.; Liu, G.; Xu, X. Bismuth and chromium codoped strontium titanates and their photocatalytic properties under visible light irradiation. *Phys. Chem. Chem. Phys.* **2015**, *17*, 26320−26329.
(14) Yu, H.; Wang, J.; Yan, S.; Yu, T.; Zou, Z. Elements doping to expand the light response of $SrTiO_3$. *J. Photochem. Photobiol., A* **2014**, *275*, 65−71.
(15) Jiao, Z.; Chen, T.; Xiong, J.; Wang, T.; Lu, G.; Ye, J.; Bi, Y. Visible-light-driven photoelectrochemical and photocatalytic performances of Cr-doped $SrTiO_3$/TiO_2 heterostructured nanotube arrays. *Sci. Rep.* **2013**, *3*, 2720.
(16) Tonda, S.; Kumar, S.; Anjaneyulu, O.; Shanker, V. Synthesis of Cr and La-codoped $SrTiO_3$ nanoparticles for enhanced photocatalytic performance under sunlight irradiation. *Phys. Chem. Chem. Phys.* **2014**, *16*, 23819−23828.
(17) Ouyang, S.; Tong, H.; Umezawa, N.; Cao, J.; Li, P.; Bi, Y.; Zhang, Y.; Ye, J. Surface-alkalinization-induced enhancement of photocatalytic H_2 evolution over $SrTiO_3$ -based photocatalysts. *J. Am. Chem. Soc.* **2012**, *134*, 1974−1977.
(18) Xie, T.-H.; Sun, X.; Lin, J. Enhanced photocatalytic degradation of RhB driven by visible light-induced MMCT of Ti(IV)-O-Fe(II) formed in Fe-doped $SrTiO_3$. *J. Phys. Chem. C* **2008**, *112*, 9753−9759.
(19) Xue, C.; Hu, S.; Chang, Q.; Li, Y.; Liu, X.; Yang, J. Fluoride doped $SrTiO_3$/TiO_2 nanotube arrays with a double layer walled structure for enhanced photocatalytic properties and bioactivity. *RSC Adv.* **2017**, *7*, 49759−49768.
(20) Kawasaki, S.; Takahashi, R.; Akagi, K.; Yoshinobu, J.; Komori, F.; Horiba, K.; Kumigashira, H.; Iwashina, K.; Kudo, A.; Lippmaa, M. Electronic structure and photoelectrochemical properties of an Ir-doped $SrTiO_3$ photocatalyst. *J. Phys. Chem. C* **2014**, *118*, 20222−20228.
(21) Zhou, X.; Shi, J.; Li, C. Effect of metal doping on electronic structure and visible light absorption of $SrTiO_3$ and $NaTaO_3$ (Metal = Mn, Fe, and Co). *J. Phys. Chem. C* **2011**, *115*, 8305−8311.
(22) Modak, B.; Ghosh, S. K. Exploring the role of La co-doping beyond charge compensation for enhanced hydrogen evolution by Rh-$SrTiO_3$. *J. Phys. Chem. B* **2015**, *119*, 11089−11098.
(23) Modak, B.; Ghosh, S. K. Role of F in improving the photocatalytic activity of Rh-doped $SrTiO_3$. *J. Phys. Chem. C* **2015**, *119*, 7215−7224.
(24) Zou, J.-P.; Zhang, L.-Z.; Luo, S.-L.; Leng, L.-H.; Luo, X.-B.; Zhang, M.-J.; Luo, Y.; Guo, G.-C. Preparation and photocatalytic activities of two new Zn-doped $SrTiO_3$ and $BaTiO_3$ photocatalysts for hydrogen production from water without cocatalysts loading. *Int. J. Hydrogen Energy* **2012**, *37*, 17068−17077.
(25) Modak, B.; Ghosh, S. K. Enhancement of visible light photocatalytic activity of $SrTiO_3$: a hybrid density functional study. *J. Phys. Chem. C* **2015**, *119*, 23503−23514.
(26) Iwashina, K.; Kudo, A. Rh-doped $SrTiO_3$ photocatalyst electrode showing cathodic photocurrent for water splitting under visible-light irradiation. *J. Am. Chem. Soc.* **2011**, *133*, 13272−13275.
(27) Kawasaki, S.; Akagi, K.; Nakatsuji, K.; Yamamoto, S.; Matsuda, I.; Harada, Y.; Yoshinobu, J.; Komori, F.; Takahashi, R.; Lippmaa, M.; Sakai, C.; Niwa, H.; Oshima, M.; Iwashina, K.; Kudo, A. Elucidation of Rh-induced in-gap states of Rh:$SrTiO_3$ visible-light-driven photocatalyst by soft X-ray spectroscopy and first-principles calculations. *J. Phys. Chem. C* **2012**, *116*, 24445−24448.
(28) Furuhashi, K.; Jia, Q.; Kudo, A.; Onishi, H. Time-resolved infrared absorption study of $SrTiO_3$ photocatalysts codoped with rhodium and antimony. *J. Phys. Chem. C* **2013**, *117*, 19101−19106.
(29) Chen, H.-C.; Huang, C.-W.; Wu, J. C. S.; Lin, S.-T. Theoretical investigation of the metal-doped $SrTiO_3$ photocatalysts for water splitting. *J. Phys. Chem. C* **2012**, *116*, 7897−7903.
(30) Kiss, B.; Manning, T. D.; Hesp, D.; Didier, C.; Taylor, A.; Pickup, D. M.; Chadwick, A. V.; Allison, H. E.; Dhanak, V. R.; Claridge, J. B.; Darwent, J. R.; Rosseinsky, M. J. Nano-structured rhodium doped SrTiO 3 -visible light activated photocatalyst for water decontamination. *Appl. Catal., B* **2017**, *206*, 547−555.
(31) Giannozzi, P.; Baroni, S.; Bonini, N.; Calandra, M.; Car, R.; Cavazzoni, C.; Ceresoli, D.; Chiarotti, G. L.; Cococcioni, M.; Dabo, I.; et al. Quantum ESPRESSO: a modular and open-source software project for quantum simulations of materials. *J. Phys.: Condens. Matter* **2009**, *21*, 395502.
(32) Perdew, J. P.; Wang, Y. Generalized gradient approximation made simpleAccurate and simple analytic representation of the electron-gas correlation energy. *Phys. Rev. B: Condens. Matter Mater. Phys.* **1992**, *45*, 13244−13249.
(33) Bantawal, H.; Shenoy, U. S.; Bhat, D. K. Tuning photocatalytic activity of SrTiO3 by varying the Sr/Ti Ratio: unusual effect of viscosity of synthetic medium. *J. Phys. Chem. C* **2018**, *122*, 20027−20033.
(34) Shenoy, S.; Bhat, D. K. Enhanced bulk thermoelectric performance of $Pb_{0.6}Sn_{0.4}Te$: effect of magnesium doping. *J. Phys. Chem. C* **2017**, *121*, 20696−20703.
(35) Mohamed, M. J. S.; Shenoy, S. U.; Bhat, D. K. Novel NRGO-CoWO4-Fe2O3 nanocomposite as an efficient catalyst for dye degradation and reduction of 4-nitrophenol. *Mater. Chem. Phys.* **2018**, *208*, 112−122.

DOI: 10.1021/acs.jpcc.8b10083
J. Phys. Chem. C 2018, 122, 27567−27574